HHS Public Access

Author manuscript

Nat Cell Biol. Author manuscript; available in PMC 2016 July 11.

Published in final edited form as:

Nat Cell Biol. 2016 February ; 18(2): 213–224. doi:10.1038/ncb3295.

The *LINK-A* lncRNA Activates Normoxic HIF1α Signaling in Triple-negative Breast Cancer

Aifu Lin[1,#], **Chunlai Li**[1,#], **Zhen Xing**[1,#], **Qingsong Hu**[1], **Ke Liang**[1], **Leng Han**[4,12], **Cheng Wang**[9], **David H. Hawke**[5], **Shouyu Wang**[1], **Yanyan Zhang**[1], **Yongkun Wei**[1], **Guolin Ma**[8], **Peter K. Park**[1], **Jianwei Zhou**[10], **Yan Zhou**[11], **Zhibin Hu**[9], **Yubin Zhou**[8], **Jeffery R. Marks**[6], **Han Liang**[4,5], **Mien-Chie Hung**[1,2,7], **Chunru Lin**[1,2,*], and **Liuqing Yang**[1,2,3,*]

[1]Department of Molecular and Cellular Oncology, The University of Texas M D Anderson Cancer Center, Houston, TX 77030

[2]The Graduate School of Biomedical Sciences, The University of Texas M D Anderson Cancer Center, Houston, TX 77030

[3]Center for RNA Interference and Non-Coding RNAs, The University of Texas M D Anderson Cancer Center, Houston, TX 77030

[4]Department of Bioinformatics and Computational Biology, Division of Quantitative Sciences, The University of Texas M D Anderson Cancer Center, Houston, TX 77030

[5]Department of System Biology, The University of Texas M D Anderson Cancer Center, Houston, TX 77030

[6]Department of Surgery, Division of Surgical Science, Duke University, School of Medicine, Durham, NC, 27710

[7]Center for Molecular Medicine and Graduate Institute of Cancer Biology, China Medical University, Taichung, 404, Taiwan

[8]Center for Translational Cancer Research, Institute of Biosciences and Technology, Texas A&M University Health Science Center, Houston, TX, 77030

[9]Department of Epidemiology and Biostatistics and Ministry of Education (MOE), School of Public Health, Nanjing Medical University

[10]Department of Molecular Cell Biology and Toxicology, School of Public Health, Nanjing Medical University, 140 Hanzhong Road, Nanjing 210029, China

[*]To whom correspondence should be addressed: ; Email: clin2@mdanderson.org and ; Email: lyang7@mdanderson.org

[12]Current address: Department of Biochemistry and Molecular Biology, University of Health Science Center at Houston Medical School, Houston, TX, 77030

[#]These authors have contributed equally.

Author Contributions

C.-R.L., L.-Q.Y. and A.-F.L. designed the research, and A.-F.L., C.-L.L. and Z.X. performed most of the experiments, with participation of K.L., S.-Y.W., Q.-S.H, Y.-Y.Z., G.-L.Ma. and Y.-B.Z. D.-H.H. executed mass spectrometry analysis. Clinical specimens were ascertained and processed by S.-Y.W., J.-W.Z., Y.Z and J.-R.M. The histological staining and corresponding analysis were performed by K.L. and Y.-K.W. P.-K.P. helped with manuscript preparation. TCGA data and microarray data analysis was performed by C.W., Z.-B.H, L.H., and H.L. M.-C.H. provided reagents and conceptual advice. L.-Q.Y., C.-R.L. and A.-F.L. wrote the manuscript.

[11]Department of Oncology, Yixing People's Hospital, 75 Zhenguan Road, Yixing 214200, China

Abstract

Although long noncoding RNAs (lncRNAs) predominately reside in nuclear and exert their functions in many biological processes, their potential involvement in cytoplasmic signal transduction remains unexplored. Here, we identified a cytoplasmic lncRNA, Long-Intergenic Noncoding RNA for Kinase Activation (*LINK-A*), which mediates HB-EGF triggered, EGFR:GPNMB heterodimer-dependent HIF1α phosphorylation at Tyr565 and Ser797 by BRK and LRRK2 respectively. These events cause HIF1α stabilization, HIF1α-p300 interaction, and activation of HIF1α transcriptional programs under normoxic conditions. Mechanistically, *LINK-A* facilitates the recruitment of BRK to EGFR:GPNMB complex and BRK kinase activation. The BRK-dependent HIF1α Tyr565 phosphorylation interferes with Pro564 hydroxylation, leading to normoxic HIF1α stabilization. Both *LINK-A* and *LINK-A*-dependent signaling pathway activation correlate with TNBC, promoting breast cancer glycolysis reprogramming and tumorigenesis. Our findings illustrate the magnitude and diversity of cytoplasmic lncRNAs in signal transduction and highlight the important roles of lncRNAs in cancer.

Keywords

Long Noncoding RNA; Triple-negative Breast Cancer (TNBC); Epidermal Growth Factor Receptor (EGFR); glycoprotein non-metastatic b (GPNMB); HIF1α; Signaling Transduction; Glycolysis Reprogramming

Introduction

Triple-Negative Breast Cancer (TNBC) continues to be a severe health problem[1–3], demanding the consideration of emerging long non-coding RNAs (lncRNAs) as biomarkers and therapeutic targets in combatting this disease[4–6]. Accumulating evidence demonstrates that lncRNAs have broad functional roles in the nucleus: regulation of transcriptional activation, X chromosome inactivation, heterochromatin formation, and maintenance of telomeres[7–14]. Alterations of these functions promote tumor formation, progression, and metastasis of many cancer types[15–20]. However, many known lncRNAs reside either within the cytosol or shuttle between the nucleus and cytoplasm[21], playing important roles in modulating messenger RNA translation, decay and cytoplasmic protein trafficking[22–24]. Intriguingly, many protein kinases and metabolic enzymes bind RNA *via* their noncanonical RNA-binding domains[25–27], raising an important question whether cytoplasmic lncRNAs are relevant in the regulation of fundamental cellular processes.

Hypoxia-Inducible Factors (HIFs)–targeted transcriptional program is involved in TNBC progression, recurrence, and metabolic reprogramming[28–30]. Although it is well known that the hydroxylation of HIF1α mediated by Proline Hydroxylase Domain (PHD) proteins triggers VHL-dependent HIF1α ubiquitination and degradation under normoxic conditions[31,32]; under certain circumstances in tumor, HIF1α can accumulate under normoxic conditions, promoting angiogenesis and cancer progression[33,34]. However, the mechanism underlying normoxic HIF1α stabilization in TNBC remains elusive.

Here, we identified a highly prognostic lncRNA in TNBC, *L*ong *I*ntergenic *N*oncoding RNA for *K*inase *A*ctivation (*LINK-A*) (also known as *LOC339535* and NR_015407), which is critical for growth factor-induced normoxic HIF1α signaling pathway. Mechanistically, *LINK-A* is required for a HB-EGF-triggered, EGFR:GPNMB heterodimer-mediated recruitment of BRK to GPNMB, and subsequent enzymatic activation of BRK. The activated BRK, together with LRRK2 that is also recruited by *LINK-A*, phosphorylate HIF1α at Tyr565 and Ser797 respectively. While the phosphorylation at Tyr565 inhibits hydroxylation at the adjacent Pro564, which prevents HIF1α degradation under normoxic conditions, Ser797 phosphorylation facilitates HIF1α-p300 interaction, leading to activation of HIF1α target genes upon HB-EGF stimulation. Furthermore, we demonstrated that LRRK2, a constitutively active kinase in Parkinson's disease, is a RNA binding kinase that phosphorylates HIF1α in human cancers. Importantly, both *LINK-A* expression and activation of the *LINK-A*-mediated normoxic HIF1a signaling pathway correlated with TNBC. Therefore, targeting *LINK-A* may serve as a favorable strategy to block a normoxic HIF1α signaling pathway in TNBC with promising therapeutic potential.

RESULTS

LINK-A is a cytoplasmic lncRNA with prognostic value for TNBC

To identify TNBC-relevant lncRNAs, we examined lncRNA expression profile in two stage III TNBC tissues and their paired adjacent noncancerous tissues, finding 21 differentially expressed lncRNAs[16]. We further searched the expression pattern of these 21 lncRNAs in the TCGA database. Interestingly, statistical analysis of a combined 711 RNA-seq transcriptome profiles indicated that the expression of *LINK-A* is frequently elevated in TNBC patient cohorts in comparison to cohorts of ERPR−/HER2+, ERPR+/HER2-, and ERPR+/HER2+ patients. Differential *LINK-A* expression between ERPR−/HER2+, ERPR+/HER2-, and ERPR+/HER2+ cohorts were not statistically significant (Fig. 1a). Consistently, basal-like breast cancer, which lacks or shows low levels of ER, PR, and HER2 proteins[35,36], exhibited significantly increased *LINK-A* expression in comparison to HER2+, LumA, LumB, and normal-like subtypes (Fig. 1b).

LINK-A is a ~1.5kb long intergenic non-protein coding RNA[37], which was confirmed by our northern blot and RACE analyses in MDA-MB-231 cells (Supplementary Fig. 1a, b). Given that *LINK-A* has a predicted ORF of 139 amino acids, we performed *in vitro* translation assays, showing that neither sense nor antisense transcript of *LINK-A* encodes protein (Supplementary Fig. 1c). We next examined *LINK-A* expression in breast cancer tissue microarrays (clinicopathological parameters listed in Supplementary Table 1) using RNAScope® 2.0 HD assay. In both training and validation sets of tissue samples, the expression of *LINK-A* was significantly increased in TNBC tissues compared to normal breast tissues, ERPR−/HER2+, ERPR+/HER2-, and ERPR+/HER2+ subtypes (Fig. 1c, d), demonstrating the strong correlation of *LINK-A* expression with TNBC. Additionally, we examined the *LINK-A* expression level in Duke breast cancer cohort, finding that high levels of *LINK-A* correlated with unfavorable recurrence free survival for breast cancer patients (Fig. 1e). Consistently, *LINK-A* was highly expressed in TNBC cell lines compared to Estrogen Receptor (ER)- or HER2-positive breast cancer cell lines (Supplementary Fig. 1d).

Next, we examined the subcellular localization of *LINK-A*, finding that *LINK-A* predominately resides in the cytoplasm or close to the cellular membrane, which was distinct from typical nuclear lncRNAs including *BCAR4*[16] and *HOTAIR*[20] (Supplementary Fig. 1e–g). Cell fractionation analysis showed that >90% of *LINK-A* is localized within the cytosolic fraction compared to the nuclear enrichment of *BCAR4* (Supplementary Fig. 1h, i). We hypothesized that *LINK-A* has important roles in the cytosol.

Identification and characterization of *LINK-A*-protein interaction

We performed an RNA pulldown assay followed by Mass Spectrometry (MS)[15,16] to identify *LINK-A*-associated proteins that might be involved in cytoplasmic processes. Interestingly, sense *LINK-A* but not antisense and beads control specifically associated with two transmembrane proteins, Epidermal Growth Factor Receptor (EGFR) and Transmembrane Glycoprotein NMB (GPNMB), tyrosine protein kinase 6 (also known as Breast Tumor Kinase, BRK)[38,39], leucine-rich repeat kinase 2 (LRRK2)[40,41], and HIF1α in the breast cancer cell (Fig. 1f, Supplementary Fig. 1j and Supplementary Table 2). RNA pulldown assay in cell lysate and RNA-protein binding assay using recombinant EGFR, BRK, LRRK2, HIF1α, and GPNMB confirmed that *LINK-A* associated with all of the proteins mentioned above *in vivo*, but only BRK and LRRK2 directly interacted with *LINK-A* (Supplementary Fig. 1k–n). The specific interaction between *LINK-A* and BRK or LRRK2 was also confirmed by an RNA immunoprecipitation (RIP) assay (Fig. 1g).

To map the BRK domains required for *LINK-A* binding, we generated BRK SH3 (a.a. 11–72), SH2 (a.a. 78–170), kinase domains (a.a. 191–445), and regulatory carboxyl-terminus (a.a. 446–451) deletion mutants (Fig. 1h, bottom panel). Deletion of either the SH3 domain or the carboxyl-terminus region of the kinase domain of BRK alone impaired the interaction between *LINK-A* and BRK, suggesting that *LINK-A* interacts with two separate domains of BRK (Supplementary Fig. 1o). Double deletion of these two domains abolished *LINK-A*-BRK interaction *in vitro* and *in vivo* (Fig. 1h and Supplementary Fig. 1p). A similar strategy was utilized to map the domain required for LRRK2-*LINK-A* interaction, showing that deletion of the WD40 domain, an atypical RNA binding domain[16,25], abolished the direct interaction (Fig. 1i and Supplementary Fig. 1q).

To map RNA motifs essential for the *LINK-A*-protein interactions, we conducted an *in vitro* RNA-protein binding coupled with dot-blot assay[15,16], finding that BRK interacted with *LINK-A* at two regions nt. 481–540 (dot B3) and nt. 781–840 (dot C2) (corresponding to the two domains of BRK at the SH3 domain and the C-terminal tail) (Fig. 1j). *LINK-A* nt. 1261–1320 (dot D4) interacted with LRRK2 (Fig. 1j). Consistently, double deletion of *LINK-A* (nt.471–550 and nt. 771–850) abolished the BRK-*LINK-A* interaction without affecting the LRRK2-*LINK-A* interaction, while deletion of *LINK-A* (nt. 1251–1330) specifically abolished LRRK2-*LINK-A* association (Fig. 1k). The predicted secondary structure of *LINK-A* indicates that the RNA motifs required for BRK and LRRK2 interactions form individual branching stem-loops, suggesting their contribution to specific RNA-protein interactions (Supplementary Fig. 1r).

Characterization of a HB-EGF-triggered, EGFR:GPNMB-dependent and *LINK-A*-mediated signaling pathway in TNBC

Our MS data revealed a series of phosphorylation sites of GPNMB (Tyr525), BRK (Tyr351), and HIF1α (Tyr565 and Ser797) (Fig. 2a, Supplementary Fig. 2a–d and Supplementary Table 2), leading us to generate phosphorylation site-specific antibodies (Supplementary Fig. 2e–i) for investigating whether *LINK-A* modulates a previously unknown signaling pathway.

Given that *LINK-A* associated with orphan receptor GPNMB and EGFR, which are involved in metastatic TNBC[42–44], we reasoned that EGFR and GPNMB may interact with each other in TNBC cells upon EGF family ligands. While all EGFR ligands effectively activated EGFR (Supplementary Fig. 2j), HB-EGF robustly induced the specific interaction between EGFR and GPNMB (Fig. 2b), indicating that EGF ligands could differentially trigger the formation of the EGFR homodimer or the heterodimer between EGFR and other receptors[45]. To test this, we performed a cross-linking assay, finding that EGF predominately triggered EGFR homodimerization with a lesser degree of EGFR:GPNMB heterodimerization while HB-EGF stimulated EGFR:GPNMB heterodimerization with less EGFR homodimerization (Fig. 2c). Knockdown of *LINK-A* exhibited minimal effects on the HB-EGF-induced EGFR:GPNMB interaction as well as GPNMB phosphorylation upon ligand stimulation (Supplementary Fig. 2k, l), suggesting that HB-EGF preferentially triggered EGFR:GPNMB heterodimer formation. We further mapped the domains mediating EGFR-GPNMB binding, and found that the kinase domain (KD) in EGFR Intracellular Domains (ICD) interacts with GPNMB ICD (Fig. 2d, e and Supplementary Fig. 2m). HB-EGF robustly induced site-specific phosphorylations of EGFR, GPNMB, BRK, and HIF1α (Fig. 2f) and pretreatment of TNBC cell lines with Cetuximab impaired EGFR-GPNMB interaction (Supplementary Fig. 2n, o). These observations led us to fully characterize this HB-EGF triggered, EGFR:GPNMB-dependent signaling pathway in TNBC.

First, an *in vitro* kinase assay indicated that EGFR, but not BRK, phosphorylated GPNMB at Tyr525 (Fig. 2g) and the exogenously expressed wild-type GPNMB but not Y525F mutant was phosphorylated *in vivo* upon HB-EGF stimulation (Fig. 2h). Next, we observed the interaction between GPNMB and BRK following ligand stimulation, which was abolished in the presence of GPNMB Y525F mutant (Fig. 2h). Furthermore, the ligand-triggered BRK Tyr351 phosphorylation was abolished in GPNMB Y525F-overexpressing cells (Fig. 2h). Biochemical experiments showed that BRK SH2 domain deletion (a.a 78–170) eliminated the ligand-dependent interaction with Tyr525-phosphorylated GPNMB (Fig. 2i). These data suggest that the EGFR-dependent GPNMB Tyr525 phosphorylation is required for further recruitment of BRK *via* its SH2 domain and subsequent phosphorylation at Tyr351.

LINK-A facilitates the recruitment and activation of BRK

We then conducted an Immuno-RNA FISH assay to examine the proximity of *LINK-A* to the ligand-bound receptors upon ligand treatment, finding the overlapping between *LINK-A* and EGFR upon HB-EGF stimulation (Supplementary Fig. 3a), which was further validated by *in vivo* RIP assay (Supplementary Fig. 3b). We examined the co-localization of BRK and EGFR:GPNMB receptor complex in the presence or absence of *LINK-A*. Our data indicate that both BRK and phospho-BRK (Tyr351) faithfully co-localized with EGFR upon HB-

EGF stimulation (Fig. 3a and Supplementary Fig. 3c). In contrast, depletion of *LINK-A* abolished the recruitment of BRK to EGFR and subsequent phosphorylation of BRK without affecting the internalization of EGFR (Fig. 3a and Supplementary Fig. 3c). we then performed rescue experiments in which *LINK-A* was knocked down by Locked Nucleic Acids (LNA) followed by re-introduction of LNA-resistant full-length *LINK-A* or one of the following deletion mutants: ΔBRK (Δ471–550 and Δ771–850) or ΔLRRK2 (Δ1251–1330) (Fig. 3b, lower panel, Supplementary Fig. 3d, e), finding that knockdown of *LINK-A* abolished the HB-EGF-induced BRK-GPNMB interaction, as well as BRK Tyr351phosphorylation (Fig. 3c, d); re-introduction of full-length *LINK-A* or ΔLRRK2 but not ΔBRK mutant rescued these phenotypes (Fig. 3c, d). These data suggest that *LINK-A*-BRK interaction facilitate the recruitment of BRK to the tyrosine phosphorylated membrane receptor GPNMB, as well as subsequent autophosphorylation of BRK.

LINK-A elicits the conformational change of BRK for kinase activation

It has been reported that the activity of BRK is auto-inhibited by interaction between the SH2 domain and the Tyr447-phosphorylated C-terminal domain[46–48]. Our data indicate that *LINK-A* interacts with BRK at two regions, SH3 domain and the C-terminal domain (see Fig. 1h and Supplementary Fig. 1p), raising a possible role of *LINK-A* in eliciting a BRK conformational change that mitigates the conformation required for self-inhibition. Indeed, we found that full-length *LINK-A* and ΔLRRK2 *LINK-A* dramatically enhanced the autophosphorylation and kinase activity of BRK while both the control lncRNA and ΔBRK *LINK-A* showed minimal effects (Fig. 3e, f).

We next conducted a protease digestion assay by incubating BRK with Caspase-1 in the presence of full-length *LINK-A* or ΔBRK *LINK-A*, finding that Caspase-1 barely cleaved BRK at aa. 397 in the presence of an unrelated lncRNA *RP11-383G10.5*, but robustly cleaved BRK only in the presence of full-length *LINK-A* (Fig. 3g), suggesting a potential conformational change occurred in BRK to expose the digestion site upon *LINK-A* binding. Notably, depletion of either two regions of *LINK-A* involved in BRK interaction failed to promote the Caspase-1 dependent BRK cleavage (Fig. 3g), suggesting that simultaneous binding of *LINK-A* to two BRK domains is required to elicit the conformational change in BRK. Our data suggest that the binding of *LINK-A* to BRK promotes a conformational change, leading to increased accessibility of the SH2 domain and the autophosphorylation sites in the kinase domain. Upon ligand stimulation, these events lead to the recruitment of BRK to Tyr525-phosphorylated GPNMB and activation of BRK upon Tyr351 phosphorylation.

LINK-A-interacting BRK and LRRK2 phosphorylate HIF1α

We next performed *in vitro* phosphorylation assays, finding that activated BRK phosphorylated HIF1α at Tyr565 (Fig. 4a) and LRRK2, another *LINK-A* interacting protein kinase, phosphorylated HIF1α at Ser797, which was further demonstrated by the marked inhibition of HIF1α phosphorylation in the presence of a S797A point mutant (Fig. 4a). The BRK kinase activity deficient mutant, Y351F, diminished the phosphorylation of HIF1α *in vivo* (Fig. 4b). Both Tyr565 and Ser797 of HIF1α are conserved (Supplementary Fig. 4a).

HB-EGF induced phosphorylation of GPNMB (Tyr525) and BRK (Tyr351), as well as HIF1α protein stabilization under normoxic conditions (Fig. 4c and Supplementary Fig. 4b). Interestingly, knockdown of EGFR abolished the ligand-dependent phosphorylation of GPNMB (Tyr525) and BRK (Tyr351), as well as the stabilization of HIF1α; knockdown of GPNMB abolished HB-EGF induced BRK phosphorylation and HIF1α protein stabilization, but did not affect EGFR phosphorylation (Tyr1068) (Fig. 4d). Knockdown of *LINK-A* in both MDA-MB-231 and MDA-MB-468 cells eliminated HB-EGF induced BRK phosphorylation and HIF1α stabilization, but not phosphorylation of EGFR or GPNMB (Fig. 4e, f). In contrast, *LINK-A* knockdown exhibited minimal effects on hypoxia-dependent HIF1α stabilization, and hypoxia failed to trigger phosphorylation of GPNMB and BRK (Fig. 4c–f and Supplementary Fig. 4c). Finally, depletion of BRK decreased ligand-triggered HIF1α protein accumulation but did not affect the phosphorylation status of EGFR or GPNMB (Fig. 4d). Taken together, these data suggest a linear EGFR:GPNMB→*LINK-A*→BRK/LRRK2→HIF1α signaling cascade upon HB-EGF stimulation under normoxic conditions.

Upon HB-EGF stimulation, HIF1α underwent Tyr565 and Ser797 phosphorylations but the hydroxylation at Pro564 was inhibited, which led to HIF1α stabilization (Fig. 4g). Knockdown of *LINK-A* abolished HB-EGF induced HIF1α Tyr565-phosphorylation and enhanced the Pro564-hydroxylation (Fig.4h and Supplementary Fig. 4d). A similar pattern was observed with EGFR, GPNMB and BRK knockdown (Fig.4i). These data suggest that HB-EGF triggers an lncRNA-dependent signaling pathway to stabilize the HIF1α at protein level.

Tyr565 phosphorylation antagonizes Pro564 hydroxylation to stabilize HIF1α under normoxia

An *in vitro* hydroxylation assay demonstrated that the HIF1α peptides (aa.557–566) but not Tyr565-phosphorylated peptides can be hydroxylated by PHD1 (Fig. 4j, Supplementary Fig. 4e–j and Supplementary Table 3). An *in vitro* kinase assay followed by *in vitro* hydroxylation assay further showed that phosphorylation of wild-type HIF1α but not Y565F mutant by BRK prevented subsequent hydroxylation at Pro564 (Fig. 4k). Consistently, HB-EGF triggered Tyr565 phosphorylation of HIF1α and inhibition of hydroxylation at Pro564, which was abolished by overexpression of the Y565F mutant of HIF1α (Fig. 4l).

Cycloheximide (CHX) treatment experiment revealed that upon HB-EGF stimulation, HIF1α protein exhibited ≥4 hours half-life while knocking down of *LINK-A* reduced it to 1.5 hours (Supplementary Fig. 4k, l). In TNBC cells exogenously expressing wild-type HIF1α or Y565D mutant, Y565D mutant exhibited constitutively prolonged half-life (Supplementary Fig. 4m–o). These data indicate that *LINK-A*-associated BRK phosphorylated HIF1α at Tyr565, which prevents HIF1α hydroxylation at adjacent Pro564 and stabilizes HIF1α under normoxia.

LINK-A-recruited LRRK2 phosphorylates Ser797 of HIF1α to potentiate its transcriptional activity

Knockdown of *LINK-A*, LRRK2, or overexpression of the HIF1α S797A mutant abolished Ser797 phosphorylation of HIF1α as well as its association with p300, which was concurrent with the release of FIH[49], a protein that binds to HIF1α and inhibits its transactivation function (Fig. 5a, b). We also examined the kinase activity of LRRK2 in the presence of *LINK-A*, finding that full-length *LINK-A*, ΔBRK *LINK-A* or ΔLRRK2 *LINK-A* exhibited minimal effect on the kinase activity of LRRK2 (Supplementary Fig. 5a). The rescue experiments indicated that full-length *LINK-A* fully rescued HIF1α phosphorylations and protein stabilization; ΔBRK *LINK-A* only rescued HIF1α Ser797 phosphorylation and ΔLRRK2 *LINK-A* restored HIF1α Tyr565 phosphorylation and protein stabilization, but failed to rescue the phosphorylation of HIF1α at Ser797 (Fig. 5c). Recent studies have shown that certain lncRNAs encode small protein peptides[50–52]. While our data have demonstrated that a predicted ORF of *LINK-A* has no protein-coding products *in vitro* (see Supplementary Fig. 1a–c), we further mutated the predicted translational start codon ATG (nt. 318–321), or the potential stop codon TGA (nt. 732–735) of this ORF in a functional rescue experiments, finding that the phosphorylation of BRK (Tyr351) and HIF1α (Tyr565), two major cellular effects mediated by *LINK-A*, were fully rescued by wild-type *LINK-A* as well as ATG→TAG or TGA→TGT mutants of *LINK-A* (Supplementary Fig. 5b–d). These observations suggested that the cellular effect of *LINK-A* is mainly dependent on its RNA function instead of the potential translational products. Taken together, we demonstrated that *LINK-A*, in coordination with two protein kinases BRK and LRRK2, mediated a growth factor-triggered signaling cascade to synergistically regulate the phosphorylation and protein stabilization of HIF1α under normoxia.

LINK-A-dependent normoxic HIF1α signaling promotes tumor growth and correlates with TNBC

Next, we examined the transcriptional activity of HIF1α upon HB-EGF stimulation by ChIP-seq, finding that under normoxia, HB-EGF triggered the recruitment of HIF1α to the promoters of HIF1α target genes and regulated the HIF1α-dependent transcriptional program (Fig. 5d, e and Supplementary Table 4). Knockdown of *LINK-A* in TNBC cells impaired HIF1α-target genes expression upon HB-EGF stimulation (Fig. 5f, g and Supplementary Fig. 5e). Consistently, *in vitro* glucose uptake and lactate production assays confirmed that *LINK-A* deficiency impaired glycolysis (Supplementary Fig. 5f–l). Consistent with the *in vitro* colony formation assays (Fig. 5h), the mice with xenografts of *LINK-A*-depleted tumor cells rarely developed tumor mass *in vivo* (Fig. 5i, j and Supplementary Fig. 5m).

LINK-A-mediated signaling pathway was also activated in TNBC tissues, as evidenced by significantly higher staining density of phospho-GPNMB (Tyr525), phospho-BRK (Tyr351), phospho-HIF1α (Tyr565), and phospho-HIF1α (Ser797) in TNBC samples compared to non-TNBC samples (Fig. 6a–c and Supplementary Fig. 6a). Furthermore, within the TNBC category, breast cancer with advanced lymph-node metastasis showed increased phospho-BRK (Tyr351), phospho-HIF1α (Tyr565), and phospho-GPNMB (Tyr525) levels compared to tissue samples with no lymph-node metastasis (Fig. 6a–c and Fig. 6d–f, upper panel).

Importantly, there is a strong correlation between *LINK-A* expression and the phosphorylation status of BRK, HIF1α, and GPNMB in these TNBC tissues (Fig. 6d–f, lower panel), and breast cancer patients with higher levels of these phosphoproteins exhibited shorter survival time (Fig. 6g–i). Furthermore, the TCGA database revealed that both BRK and LRRK2 are highly expressed in invasive breast carcinoma (Supplementary Fig. 6b). Our data implicate *LINK-A* and its associated signaling pathway as potential biomarkers and therapeutic targets for TNBC.

DISCUSSION

Our study reveals that lncRNA directly interacts with non-receptor tyrosine kinase and facilitate it's recruitment to membrane-bound receptor complex and subsequent activation upon ligand stimulation, broadening the known mechanisms of lncRNA action (Fig. 6j). The regulatory mechanism of non-receptor tyrosine kinase activation is largely unknown. We propose a model that *LINK-A* interacts with non-receptor tyrosine kinases to facilitate their activation. At the basal level, BRK, a prototype RNA-binding non-receptor tyrosine kinase, is in a "closed" conformation and its kinase activity is auto-inhibited, mediated by the self-inhibitory interaction between SH2 domain and phospho-C-terminal (Tyr447)[46]. The binding of *LINK-A* to both the SH3 domain and the C-terminal region of BRK leads to a more accessible structure of BRK as "prime" condition, which may contribute to higher accessibility by other regulatory proteins and kinases for its activation.

Most common cancer types show increased HIF1α protein levels although hypoxic areas are missing[53,54]. Our study delineates an lncRNA-protein kinase module that regulates normoxic HIF1α stabilization with respect to functional implications in the glycolytic reprogramming and tumorigenesis. The *LINK-A*-dependent HIF1α signaling cascade and the consequent effects on cancer cell glycolysis implicate *LINK-A* and *LINK-A* interacting kinases/receptors as promising therapeutic targets for TNBC. Analyses of the *LINK-A* expression status in the TCGA database and breast cancer tissues both indicated that *LINK-A* significantly correlates with TNBC, revealing an lncRNA that can serve as a biomarker for further classification of TNBC.

Our study identifies four previous unknown phosphorylation sites of GPNMB, BRK and HIF1α in a *LINK-A*-regulated signaling pathway for glycolysis reprogramming in TNBC. These phosphorylation events predict worse outcome in TNBC patients, suggesting that *LINK-A*-dependent signaling pathway plays a critical role in TNBC and may provide wide-ranging therapeutic targets for treating TNBC.

Methods

Tissue samples

Breast cancer tissue microarrays were purchased from Biomax, Biochain and USbiolabs. Two sets of fresh frozen breast cancer tissues (Nanjing Cohorts and Duke Cohorts) were obtained from Yixing People's Hospital (Yixing, Jiangsu Province, China) and Duke University respectively. The study protocol was approved by the Institutional Review Board of Nanjing Medical University (Nanjing, China) and Duke University Health System. All

tissue samples were collected in compliance with informed consent policy. Detailed clinical information is summarized in Supplementary Table 1.

Cell culture, transfection, and lentiviral transduction

Human Breast cancer cell lines, human mammary gland epithelia cell line, and human embryonic kidney cell line were purchased from American Type Culture Collection (ATCC) and Characterized Cell Line Core Facility (MD Anderson Cancer Center). siRNA and plasmid transfections were performed using DharmaFECT4 (Thermo Scientific) and Lipofectamine® 3000 (Life Technologies). Lentiviruses were produced in HEK293T cells with ViraPower Lentiviral Expression System. All of the cell lines were free of mycoplasma contamination tested by vendors using MycoAlert kit from Lonza. No cell lines used in this study are found in the database of commonly misidentified cell lines (ICLAC and NCBI Biosample) based on short tandem repeats (STR) profiling performed by vendors.

Cell treatments, cross-linking, fractionation, cell lysis, immunoprecipitation and immunoblotting

Cells were serum starved overnight followed by growth factor (Peprotech) treatment for 30 minutes at the following concentrations: EGF (10 ng/ml), Amphiregulin (10 ng/ml), Betacellulin (10 ng/ml), Epigen (200 ng/ml), Epiregulin (10 ng/ml), HB-EGF (10 ng/ml), Heregulin-β1 (5 ng/ml), TGF-α (2 ng/ml). Cetuximab (20 μg/ml) was provided by Dr. Scott Kopetz (MD Anderson Cancer Center). Chemical cross-linking was carried out as previously described[55] with 1 mM 3,3´-Dithiobis[sulfosuccinimidylpropionate] (DTSSP) (Pierce). In certain experiments, cells were pre-treated with 10 μM InSolution™ MG-132 (EMD Millipore) for 6 hours before growth factor treatment. Nuclear /cytoplasmic fractionation, cell lysis, immunoprecipitation and immunoblotting were performed as previously described[16].

RNA preparation, northern blot and RACE analysis

RNA *in vitro* transcription and purification were performed as previously described[16]. Total RNAs from 1×10^6 MDA-MB-231 cells with or without HB-EGF treatment were analyzed for *LINK-A* and *Beta-Actin* expression using Biotin-labeled LNA™ probes (Exiqon, sequence are listed in the **Oligonucleotide sequences, probes and primers section**) according to NorthernMax® Kit (Ambion). RACE-PCR was performed using SMARTer RACE 5'/3' Kit (Clontech).

Cloning procedures

Full-length *LINK-A* and deletion mutants were constructed by subcloning the gene sequences into pCDNA3.1 (+) backbone (Life Technologies). To generate LNA#5-resistant *LINK-A* mammalian expression vectors used in the rescue experiments, LNA#5 targeting sequence ACA GCT CAT TTA TCC A was mutated to ACA GGC GAT TTA TCC A.

The full-length HIF1α, GPNMB, BRK and LRRK2 mammalian expression vectors were obtained from Origene and Addgene. His-tagged full-length EGFR, extracellular domain (ECD) and intracellular domain (ICD) were provided by Dr. Mien-Chie Hung (MD Anderson Cancer Center). FLAG-tagged full-length GPNMB, ECD+transmembrane domain

(TM), and ICD+TM were constructed by subcloning the corresponding gene sequences into SFB-tagged expression vector (provided by Dr. Junjie Chen, MD Anderson Cancer Center) using the Gateway system (Life Technologies).

Bacterial expression vectors for His-tagged HIF1α and GPNMB ICD were constructed by subcloning the corresponding gene sequences into pET-DEST42 vector. GST-tagged BRK (wt and mutants) were constructed into pGEX-5X-1 backbone (GE Healthcare). GST-tagged EGFR ICD, EGFR kinase domain (KD), and EGFR C-terminal domain (CTD) in pGEX-6p-1backbone were provided by Dr. Mien-Chie Hung (MD Anderson Cancer Center).

All single-point and deletion mutations were generated using QuikChange™ Lightning Site-Directed Mutagenesis Kit (Agilent Technologies).

siRNA, shRNA and LNA™

Lincode SMARTpool siRNA targeting *LINK-A* (R-027622) and ON-TARGETplus SMARTpool siRNA targeting *EGFR* (L-003114), *GPNMB* (L-011741), *PTK6/BRK* (L-003166) and *LRRK2* (L-006323) from Dharmacon were used in this study. shRNA targeting *LINK-A* was designed based on Lincode SMARTpool siRNA sequence and cloned into pLKO.1-Puro vector. LNAs targeting *LINK-A* were designed and synthesized by Exiqon. Detailed sequences were listed in **Oligonucleotide sequences, probes and primers** section.

Antibodies

Cell Signaling Technology: anti-EGFR (D38B1) rabbit mAb (4267), anti-GPNMB (E1Y7J) rabbit mAb (13251), anti-LRRK2 (5559), anti-phospho-EGFR (Tyr845) (D63B4) rabbit mAb (6963), anti-phospho-EGFR (Tyr992) (2235), anti-phospho-EGFR (Tyr1045) (2237), anti-phospho-EGFR (Tyr1068) (D7A5) rabbit mAb (3777), anti-phospho-EGFR (Tyr1148) (4404), anti-phospho-EGFR (Tyr1173) (53A5) rabbit mAb (4407), anti-hydroxy-HIF1α (Pro564) (D43B5) rabbit mAb (3434), anti-PHD2 (3293), anti-VHL (2738), anti-LRRK2 (5559), anti-EGFR (D38B1) rabbit mAb (Alexa Fluor® 555 Conjugate) (5108), anti-GST tag (26H1) mouse mAb (2624), anti-His tag (2365) and anti-eIF4B (3592); Santa Cruz Biotechnology: anti-FIH (H-299) (sc-48813), anti-HA (Y-11) (sc-805), anti-BRK (C-18) (sc-1118), anti-GAPDH (6C5) mouse mAb (sc-32233) and anti-HIF1α (28b) mouse mAb (sc-13515); Millipore: anti-phosphotyrosine (4G10) Platinum mouse mAb (05-1050X), anti-Myc tag (4A6) mouse mAb (05-724) and anti-eIF4B (ABS281); Thermo Scientific: anti-EGFR (Ab-13) mouse mAb (MS-609); Sigma-Aldrich: anti-FLAG tag (M2) mouse mAb (F3165); Active Motif: anti-p300 (NM11) mouse mAb (61402); Novus Biologicals: anti-HIF1α (NB100-134); Life Technologies: anti-phosphoserine (Poly-Z-PS1); YenZym Antibodies, LLC: anti-phospho-GPNMB (Tyr525) [p-GPNMB (Tyr525)], anti-phospho-BRK (Tyr351) [p-BRK (Tyr351)], anti-phospho-HIF1α (Tyr565) [p-HIF1α (Tyr565)], and anti-phospho-HIF1α (Ser797) [p-HIF1α (Ser797)]. The specificity of phospho-specific antibodies were confirmed by blocking peptide competition assay. The antibodies were used as 1:1000 dilutions for immunoblotting experiments and 1:200 for immunoprecipitation, immunofluorescence and immunohistochemistry experiments.

Protein recombination, purification and *in vitro* translation

Recombinant proteins were expressed in *E.coli* strain BL21-CodonPlus® (DE3)-RIPL (Agilent Technologies) and purified using Protein Purification Kit (Clontech). Recombinant Flag-GPNMB and PHD1 were purchased from Origene. GST-EGFR was purchased from Active Motif, HIF1α and BRK were purchased from Novus Biologicals. LRRK2 was purchased from SignalChem. Recombinant active Caspase-1 was purchased from R&D Systems. *In vitro* translation of *LINK-A* was conducted using TnT® Quick Coupled Transcription/Translation Kit and detection was performed using Transcend™ Non-Radioactive Translation Detection System (Promega).

RNA pulldown, mass spectrometry analysis, *in vitro* RNA-protein binding assay and *in vitro* RNA-protein binding coupled with dot-blot assay

The cell lysates were freshly prepared using ProteaPrep Zwitterionic Cell Lysis Kit, Mass Spec Grade (Protea®) with Anti-RNase, Protease/ Phosphatase Inhibitor Cocktail, Panobinostat and Methylstat supplemented in the lysis buffer. The BcMag™ Monomer avidin Magnetic Beads (Bioclone) were first prepared according to manufacturer's instructions and then immediately subjected to RNA (20 μg) capture in RNA capture buffer [20 mM Tris-HCl pH 7.5, 1M NaCl, 1mM EDTA] for 30 minutes at room temperature with agitation. The RNA-captured beads were washed once with NT2 buffer [50 mM Tris-HCl pH 7.4, 150 mM NaCl, 1 mM $MgCl_2$, 0.05% NP-40] and incubated with 30 mg cell lysates diluted in NT2 buffer supplemented with 50 U/mL Anti-RNase, 2 mM dithiothreitol, 30 mM EDTA and Heparin 0.02 mg/ml for 4 hours at 4°C with rotation. The RNA-binding protein complexes were washed sequentially with NT2 buffer (twice), NT2-high salt buffer containing 500 mM NaCl (twice), NT2-high salt buffer containing 1 M NaCl (once), NT2-KSCN buffer containing 750 mM KSCN (twice) and PBS (once) for 5 minutes at 4°C and eluted by 2 mM D-biotin in PBS. The eluted protein complexes were denatured, reduced, alkylated and digested with immobilized trypsin (Promega) for MS analysis at MD Anderson Cancer Center Proteomics Facility. The RNA-protein binding assays and *in vitro* RNA-protein binding coupled with dot-blot assay were performed as described previously[16].

RNAScope® assay, RNA FISH, immunofluorescence and immunohistochemistry

RNAScope® assay and RNA FISH were performed as previously described[16]. RNAScope® robes targeting *LINK-A* (Cat# 412027), *BCAR4* (Cat# 407777) or *HOTAIR* (Cat# 312347) were custom designed or purchased from Advanced Cell Diagnostics. LNA™ FISH probes targeting *LINK-A* and control probe targeting *Beta-Actin* (300512-04) were purchased from Exiqon (sequences were listed in **Oligonucleotide sequences, probes and primers** section).

For immuno-RNA FISH, the slide from RNA FISH was further blocked with blocking buffer [1 × PBS, 5% BSA, 0.3% Triton X-100] for 1 hour at room temperature followed by incubation with primary antibodies (diluted 1:200) for 1 hour at room temperature. After incubation with fluorochrome-conjugated secondary antibodies for 1 hour at room temperature in dark, the slide was washed and mounted for detection. Immunofluorescence and immunohistochemistry were performed as previously described[16].

The quantification of RNAScope® staining densities was measured by RNAscope® SpotStudio v1.0 Software (Advanced Cell Diagnostics). The quantification of IHC staining density was performed by Image-Pro plus 6.0 (Media Cybernetics) and calculated based on the average staining intensity and the percentage of positively stained cells.

Computational analysis of TCGA RNA-Seq data

Breast cancer RNA-seq BAM files was downloaded from UCSC Cancer Genomics Hub (CGHub, https://cghub.ucsc.edu/). TCGA BAM files were generated based on MapSplice algorithm for alignment against the hg19 reference genome using default parameters[56]. We then quantified lncRNA expression *LINK-A* as RPKM (reads per kilobase per million mapped reads)[57] as previously described[58], and the analysis was based on $\log_2$(RPKM+1). Clinical information, PAM50 subtype, ER, PR, and HER2 status, were obtained from the TCGA marker paper[1]. We used analysis of variance (ANOVA) or student t-test to detect the statistical difference between two or more groups.

In vitro kinase assay

Wild-type or mutant substrate proteins were incubated with 50 μl of *in vitro* kinase assay buffer II (SignalChem) containing 100 μM ATP (cold reaction) or 10 μCi [γ-^{32}P] ATP and indicated protein kinase for 1 hour at 30°C. Resulting products were separated by SDS-PAGE and detected by Coomassie Blue staining, autoradiography or immunoblotting with phospho-specific antibodies. The specific BRK and LRRK2 kinase activity were measured using a Universal Kinase Activity Kit (R&D Systems).

In vitro HIF1α hydroxylation assay

Five μg wild-type His-tagged HIF1α or Y565F mutant was incubated with 1 μg recombinant PHD1 in a reaction buffer containing 10 μM $FeSO_4$, 100 μM 2-oxo-glutarate, 1 mM ascorbate, 100 μM dithiothreitol, and 50 μM Tris-HCl (pH 7.8) at 37°C for 1 hour. HIF1α hydroxylation was analyzed by SDS-PAGE and immunoblotting with specific antibody against Pro564 hydroxylation. For the quantitative peptide hydroxylation assay, 10 μg synthesized unmodified peptide (LDLEMLAPYI) or Tyr565-phosphopeptide (LDLEMLAP-pY-I) and 3 μg recombinant PHD1 were incubated in the same reaction buffer described above or in the same buffer, except containing 100 μM DMOG. Resulting peptides were purified by ZipTip and analyzed by liquid chromatography coupled with tandem MS (LC-MS) to confirm the presence of the Proline-hydroxylated peptides. The acquired MS/MS data were searched against a database to identify hydroxylated Proline sites through a dynamic mass shift for the modified Proline (+15.9949 Da).

Chromatin immunoprecipitation (ChIP), RNA immunoprecipitation (RIP), ChIP-seq and data analysis

ChIP and RIP were performed as previously described[16]. ChIP-seq and data analysis were performed by ArrayStar. The mapped reads were used for peak detection by MACS v1.4.0 (Model-based Analysis of ChIP-Seq) software. Statistically significant ChIP-enriched regions (peaks) were identified by comparison to a Poisson background model (Cut-off *p*-value=10^{-4}).

Anchorage-independent growth assay, glucose uptake assay and lactate production assay

Anchorage-independent growth assay was performed as previously described[59]. Glucose uptake and lactate production assay were performed using Glucose Uptake Cell-based Assay Kit and L-Lactate Assay Kit (Cayman Chemical) respectively. Lactate production was expressed as lactate concentration *per* 10^4 viable cells.

In vivo tumorigenesis study

All animal experiments were performed in accordance with a protocol approved by the Institutional Animal Care and Use Committee of MD Anderson Cancer Center. Animals arrived in our facility were randomly put into cages with five mice each. They were implanted with respective tumor cells in the unit of cages, which were randomly selected. The animal experiment was set up to use 5 mice *per* group to detect a 2-fold difference with power of 80% and at the significance level of 0.05 by a two-sided test for significant studies. Tumor cells in 30 μl growth medium (mixed with Matrigel at a 1:1 ratio) were injected subcutaneously into the flank of six- to eight-week-old female nude mice. Tumor size was measured every five days using a caliper, and tumor volume was calculated using the standard formula: $0.54 \times L \times W^2$, where L is the longest diameter and W is the shortest diameter. The tumors were removed, photographed and weighed. The investigators were not blinded to allocation during experiments and outcome assessment.

Oligonucleotide sequences (5'-3'), probes (5'-3') and primers (forward and reverse)

qPCR primers for gene expression and RIP—*LINK-A* (TTC CCC CAT TTT TCC TTT TC and CTC TGG TTG GGT GAC TGG TT); *GAPDH* (GAA GGT GAA GGT CGG AGT and GAA GAT GGT GAT GGG ATT TC); *ANGPTL4* (CAC AGC CTG CAG ACA CAA CT and AAA CTG GCT TTG CAG ATG CT); *ALDOA* (CTG CCA GTA TGT GAC CGA GA and ACA GGA AGG TGA TCC CAG TG); *ANKRD37* (GTA GCC AGT GAT GCC CAA AT and CTT CCG AGA CTC CGT TTC TG); *BHLHE40* (CCT TGA AGC ATG TGA AAG CA and GCT TGG CCA GAT ACT GAA GC); *EGR1* (TGA CCG CAG AGT CTT TTC CT and TGG GTT GGT CAT GCT CAC TA); *IGFBP3* (GGG GTG TAC ACA TTC CCA AC and AGG CTG CCC ATA CTT ATC CA); *LDHA* (TGT GCC TGT ATG GAG TGG AA and AGC ACT CTC AAC CAC CTG CT); *MAPK1* (CCA GAG AAC CCT GAG GGA GA and TCG ATG GTT GGT GCT CGA AT); *PKM2* (ATC GTC CTC ACC AAG TCT GG and GAA GAT GCC ACG GTA CAG GT); *RPLP0* (TGG TCA TCC AGC AGG TGT TCG A and ACA GAC ACT GGC AAC ATT GCG G); *HIF1α* (GTC TGA GGG GAC AGG AGG AT and CTC CTC AGG TGG CTT GTC AG); *B2M* (GGC TAT CCA GCG TAC TCC AA and TGG ATG AAA CCC AGA CAC ATA)

qPCR primers for *LINK-A* knockdown-rescue gene expression and RIP experiments—*LINK-A* (TAT GGA GGA TCG CTG TTT CC and CCA AAG ATG TCG CAG GAC TT)

siRNA sequences—*LINK-A* (UGU CUA AGG UGG AGA UUA C, AGA UGU AGU UCU AGU UCA U, UUA CUG AGG UUG AAU AUG U and GGU CUU CAU UCU UAC GCU U); *EGFR* (CAA AGU GUG UAA CGG AAU A, CCA UAA AUG CUA CGA AUA U, GUA ACA AGC UCA CGC AGU U, and CAG AGG AUG UUC AAU AAC U);

GPNMB (GGA AUU UCA UCU ACG UCU U, AUA UAA CAU UUG CGG UGA A, UGC AAG AAG AGG CGG GAU A, and CCA GAA GAA CGA UCG AAA U); *PTK6/BRK* (GAG AAA GUC CUG CCC GUU U, CCA UUA AGG UGA UUU CUC G, UGC CCG AGC UUG UGA ACU A, and GGC CAU UAC UCC ACC AAA U), *LRRK2* (CAA GUU AUU UCA AGG CAA A, UUA CCG AGA UGC CGU AUU A, GGA GGG AUC UUC UUU AAU U, and GAA AUU AUC AUC CGA CUA U)

LNA™ GapmeR sequences—Negative control (AAC ACG TCT ATA CGC); *LINK-A* #1 (GCG TAA GAA TGA AGA); *LINK-A* #2 (GTG ATA AGA CTA AGT G); *LINK-A* #3(GAA TAA GGA TAA GCG T); *LINK-A* #4 (CCA CAG CTT GAA TTC C) and *LINK-A* #5(TGG ATA AAT GAG CTG T)

LINK-A* shRNA sequences—LINK-A* sh#1 (TGT CTA AGG TGG AGA TTA C); *LINK-A* sh#2 (AGA TGT AGT TCT AGT TCA T); *LINK-A* sh#3 (TTA CTG AGG TTG AAT ATG T); *LINK-A* sh#4 (GGT CTT CAT TCT TAC GCT T).

RNA FISH probes—*LINK-A* (/56-FAM/TGT AGC CAC AGA CAT CAT TAC A), *beta-Actin* (/Fluorescein/CTC ATT GTA GAA GGT GTG GTG CCA).

LNA™ RNA detection probes—*Beta-Actin* (/5Biosg/CTC ATT GTA GAA GGT GTG GTG CCA) and *LINK-A* (/5Biosg/ ACT AAG TGT TGG CAG GTT ATG T).

***LINK-A* RACE-PCR primers—**3'-RACE (TGG AAT TCA AGC TGT GGG TG) and 5'-RACE (GCA TTT TTA TTT TAA TTG AGG)

qPCR primers for ChIP—EGLN3 (CGT GGA GGA CTG GCT CTA AG and GGT GTG CTC GGG TGT G)[60], ERRFI1 (GAT TAC AGG CTG GAT GGC AC and TGC TGC CAG ACT GGT ATG AG)[61], ARRDC3 (CCC CTG CAG TCA CAC ACT C and TTT GTC ACA TGG GAC TCT TC)[31], ANKRD37 (CCA GTT TCC TGG TTA CGT GC and TAA GTC AGT GGG CGT GAG AG)[62], RPLP0 (TGA AGA GCA GAG GCG ACC CAC and ATG GGT GTC GGC GTG AC)[60].

Statistics & Reproducibility

The experiment was set up to use 3–5 samples/repeats *per* experiment/group/condition to detect a 2-fold difference with power of 80% and at the significance level of 0.05 by a two-sided test for significant studies. For RNAscope®, immunostaining, immunohistochemical staining, colony formation assay, northern blotting, RACE analysis, and western blotting, the representative images are shown. Each of these experiments was independently repeated for 3–5 times. Relative quantities of gene expression level were normalized to *B2M*. The relative quantities of ChIP samples were normalized by individual inputs, respectively. Results are reported as mean ± standard error of the mean (S.E.M.) of at least three independent experiments. Each exact n value is indicated in the corresponding figure legend. Comparisons were performed using two tailed paired Student's t test or two-way ANOVA (*$p < 0.05$, **$p < 0.01$, and ***$p < 0.001$), as indicated in individual figures. Fisher's exact test was implemented for statistical analyses of the correlation between markers and clinical parameters. For survival analysis, the expression of *LINK-A* or phosphorylation density of

indicated proteins was treated as a binary variant and divided into 'high' and 'low' level. Kaplan-Meier survival curves were compared using the Gehan-Breslow test with GraphPad Prism (GraphPad Software). The experiments were not randomized. The investigators were not blinded to allocation during experiments and outcome assessment.

Supplementary Material

Refer to Web version on PubMed Central for supplementary material.

Acknowledgments

We thank D. Aten for assistance with figure presentation. This work was supported by NIH R00 award (R00DK094981), UT Startup and UT STARS grants to C.-R.L., and the NIH R00 award (R00CA166527), CPRIT award (R1218), UT Startup and UT STARS grants to L.-Q.Y.

References

1. Cancer Genome Atlas, N. Comprehensive molecular portraits of human breast tumours. Nature. 2012; 490:61–70. [PubMed: 23000897]
2. Foulkes WD, Smith IE, Reis-Filho JS. Triple-negative breast cancer. N Engl J Med. 2010; 363:1938–1948. [PubMed: 21067385]
3. Hudis CA, Gianni L. Triple-negative breast cancer: an unmet medical need. Oncologist. 2011; 16(Suppl 1):1–11. [PubMed: 21278435]
4. Prensner JR, Chinnaiyan AM. The emergence of lncRNAs in cancer biology. Cancer Discov. 2011; 1:391–407. [PubMed: 22096659]
5. Cheetham SW, Gruhl F, Mattick JS, Dinger ME. Long noncoding RNAs and the genetics of cancer. Br J Cancer. 2013; 108:2419–2425. [PubMed: 23660942]
6. Gutschner T, Diederichs S. The hallmarks of cancer: a long non-coding RNA point of view. RNA biology. 2012; 9:703–719. [PubMed: 22664915]
7. Lee JT. Epigenetic regulation by long noncoding RNAs. Science. 2012; 338:1435–1439. [PubMed: 23239728]
8. Rinn JL, Chang HY. Genome regulation by long noncoding RNAs. Annu Rev Biochem. 2012; 81:145–166. [PubMed: 22663078]
9. Batista PJ, Chang HY. Long noncoding RNAs: cellular address codes in development and disease. Cell. 2013; 152:1298–1307. [PubMed: 23498938]
10. Morlando M, Ballarino M, Fatica A, Bozzoni I. The Role of long noncoding RNAs in the epigenetic control of gene expression. ChemMedChem. 2014; 9:505–510. [PubMed: 24488863]
11. Orom UA, Derrien T, Guigo R, Shiekhattar R. Long noncoding RNAs as enhancers of gene expression. Cold Spring Harb Symp Quant Biol. 2010; 75:325–331. doi:sqb.2010.75.058 [pii] 10.1101/sqb.2010.75.058. [PubMed: 21502407]
12. Ponting CP, Oliver PL, Reik W. Evolution and functions of long noncoding RNAs. Cell. 2009; 136:629–641. doi:S0092-8674(09)00142-1 [pii] 10.1016/j.cell.2009.02.006. [PubMed: 19239885]
13. Vance KW, Ponting CP. Transcriptional regulatory functions of nuclear long noncoding RNAs. Trends Genet. 2014; 30:348–355. [PubMed: 24974018]
14. Wang X, Song X, Glass CK, Rosenfeld MG. The long arm of long noncoding RNAs: roles as sensors regulating gene transcriptional programs. Cold Spring Harb Perspect Biol. 2011; 3:a003756. a003756 [pii] cshperspect.a003756 [pii]. [PubMed: 20573714]
15. Yang L, et al. lncRNA-dependent mechanisms of androgen-receptor-regulated gene activation programs. Nature. 2013; 500:598–602. [PubMed: 23945587]
16. Xing Z, et al. lncRNA Directs Cooperative Epigenetic Regulation Downstream of Chemokine Signals. Cell. 2014; 159:1110–1125. [PubMed: 25416949]

17. Yuan JH, et al. A long noncoding RNA activated by TGF-beta promotes the invasion-metastasis cascade in hepatocellular carcinoma. Cancer Cell. 2014; 25:666–681. [PubMed: 24768205]
18. Prensner JR, et al. The long noncoding RNA SChLAP1 promotes aggressive prostate cancer and antagonizes the SWI/SNF complex. Nat Genet. 2013; 45:1392–1398. [PubMed: 24076601]
19. Trimarchi T, et al. Genome-wide Mapping and Characterization of Notch-Regulated Long Noncoding RNAs in Acute Leukemia. Cell. 2014; 158:593–606. [PubMed: 25083870]
20. Gupta RA, et al. Long non-coding RNA HOTAIR reprograms chromatin state to promote cancer metastasis. Nature. 2010; 464:1071–1076. doi:nature08975 [pii] 10.1038/nature08975. [PubMed: 20393566]
21. Mercer TR, Mattick JS. Structure and function of long noncoding RNAs in epigenetic regulation. Nat Struct Mol Biol. 2013; 20:300–307. [PubMed: 23463315]
22. Carrieri C, et al. Long non-coding antisense RNA controls Uchl1 translation through an embedded SINEB2 repeat. Nature. 2012; 491:454–457. [PubMed: 23064229]
23. Wang P, et al. The STAT3-binding long noncoding RNA lnc-DC controls human dendritic cell differentiation. Science. 2014; 344:310–313. [PubMed: 24744378]
24. Yoon JH, Abdelmohsen K, Gorospe M. Posttranscriptional gene regulation by long noncoding RNA. J Mol Biol. 2013; 425:3723–3730. [PubMed: 23178169]
25. Castello A, et al. Insights into RNA biology from an atlas of mammalian mRNA-binding proteins. Cell. 2012; 149:1393–1406. [PubMed: 22658674]
26. Ciesla J. Metabolic enzymes that bind RNA: yet another level of cellular regulatory network? Acta biochimica Polonica. 2006; 53:11–32. [PubMed: 16410835]
27. Lunde BM, Moore C, Varani G. RNA-binding proteins: modular design for efficient function. Nat Rev Mol Cell Biol. 2007; 8:479–490. [PubMed: 17473849]
28. Semenza GL. Targeting HIF-1 for cancer therapy. Nat Rev Cancer. 2003; 3:721–732. [PubMed: 13130303]
29. Denko NC. Hypoxia, HIF1 and glucose metabolism in the solid tumour. Nat Rev Cancer. 2008; 8:705–713. [PubMed: 19143055]
30. Wong CC, et al. Hypoxia-inducible factor 1 is a master regulator of breast cancer metastatic niche formation. Proc Natl Acad Sci U S A. 2011; 108:16369–16374. [PubMed: 21911388]
31. Ivan M, et al. HIFalpha targeted for VHL-mediated destruction by proline hydroxylation: implications for O2 sensing. Science. 2001; 292:464–468. [PubMed: 11292862]
32. Min JH, et al. Structure of an HIF-1alpha -pVHL complex: hydroxyproline recognition in signaling. Science. 2002; 296:1886–1889. [PubMed: 12004076]
33. Knowles HJ, Mole DR, Ratcliffe PJ, Harris AL. Normoxic stabilization of hypoxia-inducible factor-1alpha by modulation of the labile iron pool in differentiating U937 macrophages: effect of natural resistance-associated macrophage protein 1. Cancer Res. 2006; 66:2600–2607. [PubMed: 16510578]
34. Kuschel A, Simon P, Tug S. Functional regulation of HIF-1alpha under normoxia--is there more than post-translational regulation? J Cell Physiol. 2012; 227:514–524. [PubMed: 21503885]
35. Livasy CA, et al. Phenotypic evaluation of the basal-like subtype of invasive breast carcinoma. Mod Pathol. 2006; 19:264–271. [PubMed: 16341146]
36. Badve S, et al. Basal-like and triple-negative breast cancers: a critical review with an emphasis on the implications for pathologists and oncologists. Mod Pathol. 2011; 24:157–167. [PubMed: 21076464]
37. Bubb KL, et al. Scan of human genome reveals no new Loci under ancient balancing selection. Genetics. 2006; 173:2165–2177. [PubMed: 16751668]
38. Regan Anderson TM, et al. Breast tumor kinase (Brk/PTK6) is a mediator of hypoxia-associated breast cancer progression. Cancer Res. 2013; 73:5810–5820. [PubMed: 23928995]
39. Miah S, Martin A, Lukong KE. Constitutive activation of breast tumor kinase accelerates cell migration and tumor growth in vivo. Oncogenesis. 2012; 1:e11. [PubMed: 23552639]
40. Agalliu I, et al. Higher frequency of certain cancers in LRRK2 G2019S mutation carriers with Parkinson disease: a pooled analysis. JAMA neurology. 2015; 72:58–65. [PubMed: 25401981]

41. Martin I, et al. Ribosomal protein s15 phosphorylation mediates LRRK2 neurodegeneration in Parkinson's disease. Cell. 2014; 157:472–485. [PubMed: 24725412]
42. Rose AA, et al. Glycoprotein nonmetastatic B is an independent prognostic indicator of recurrence and a novel therapeutic target in breast cancer. Clin Cancer Res. 2010; 16:2147–2156. [PubMed: 20215530]
43. Ueno NT, Zhang D. Targeting EGFR in Triple Negative Breast Cancer. Journal of Cancer. 2011; 2:324–328. [PubMed: 21716849]
44. Maric G, et al. GPNMB cooperates with neuropilin-1 to promote mammary tumor growth and engages integrin alpha5beta1 for efficient breast cancer metastasis. Oncogene. 2015; 34:5494–5504. [PubMed: 25772243]
45. Saito Y, Haendeler J, Hojo Y, Yamamoto K, Berk BC. Receptor heterodimerization: essential mechanism for platelet-derived growth factor-induced epidermal growth factor receptor transactivation. Mol Cell Biol. 2001; 21:6387–6394. [PubMed: 11533228]
46. Qiu H, Miller WT. Regulation of the nonreceptor tyrosine kinase Brk by autophosphorylation and by autoinhibition. J Biol Chem. 2002; 277:34634–34641. [PubMed: 12121988]
47. Kamalati T, et al. Brk, a breast tumor-derived non-receptor protein-tyrosine kinase, sensitizes mammary epithelial cells to epidermal growth factor. J Biol Chem. 1996; 271:30956–30963. [PubMed: 8940083]
48. Brauer PM, Tyner AL. Building a better understanding of the intracellular tyrosine kinase PTK6 - BRK by BRK. Biochim Biophys Acta. 2010; 1806:66–73. [PubMed: 20193745]
49. Mahon PC, Hirota K, Semenza GL. FIH-1: a novel protein that interacts with HIF-1alpha and VHL to mediate repression of HIF-1 transcriptional activity. Genes Dev. 2001; 15:2675–2686. [PubMed: 11641274]
50. Andrews SJ, Rothnagel JA. Emerging evidence for functional peptides encoded by short open reading frames. Nat Rev Genet. 2014; 15:193–204. [PubMed: 24514441]
51. Ruiz-Orera J, Messeguer X, Subirana JA, Alba MM. Long non-coding RNAs as a source of new peptides. eLife. 2014; 3:e03523. [PubMed: 25233276]
52. Anderson DM, et al. A micropeptide encoded by a putative long noncoding RNA regulates muscle performance. Cell. 2015; 160:595–606. [PubMed: 25640239]
53. Stroka DM, et al. HIF-1 is expressed in normoxic tissue and displays an organ-specific regulation under systemic hypoxia. FASEB J. 2001; 15:2445–2453. [PubMed: 11689469]
54. Schwab LP, et al. Hypoxia-inducible factor 1alpha promotes primary tumor growth and tumor-initiating cell activity in breast cancer. Breast cancer research : BCR. 2012; 14:R6. [PubMed: 22225988]

References

55. Yu X, Sharma KD, Takahashi T, Iwamoto R, Mekada E. Ligand-independent dimer formation of epidermal growth factor receptor (EGFR) is a step separable from ligand-induced EGFR signaling. Mol Biol Cell. 2002; 13:2547–2557. [PubMed: 12134089]
56. Wang K, et al. MapSplice: accurate mapping of RNA-seq reads for splice junction discovery. Nucleic Acids Res. 2010; 38:e178. [PubMed: 20802226]
57. Mortazavi A, Williams BA, McCue K, Schaeffer L, Wold B. Mapping and quantifying mammalian transcriptomes by RNA-Seq. Nature methods. 2008; 5:621–628. [PubMed: 18516045]
58. Han L, et al. The Pan-Cancer analysis of pseudogene expression reveals biologically and clinically relevant tumour subtypes. Nat Commun. 2014; 5:3963. [PubMed: 24999802]
59. Borowicz S, et al. The soft agar colony formation assay. Journal of visualized experiments : JoVE. 2014:e51998. [PubMed: 25408172]
60. Ortiz-Barahona A, Villar D, Pescador N, Amigo J, del Peso L. Genome-wide identification of hypoxia-inducible factor binding sites and target genes by a probabilistic model integrating transcription-profiling data and in silico binding site prediction. Nucleic Acids Res. 2010; 38:2332–2345. [PubMed: 20061373]
61. Schodel J, et al. High-resolution genome-wide mapping of HIF-binding sites by ChIP-seq. Blood. 2011; 117:e207–e217. [PubMed: 21447827]

62. Benita Y, et al. An integrative genomics approach identifies Hypoxia Inducible Factor-1 (HIF-1)-target genes that form the core response to hypoxia. Nucleic Acids Res. 2009; 37:4587–4602. [PubMed: 19491311]

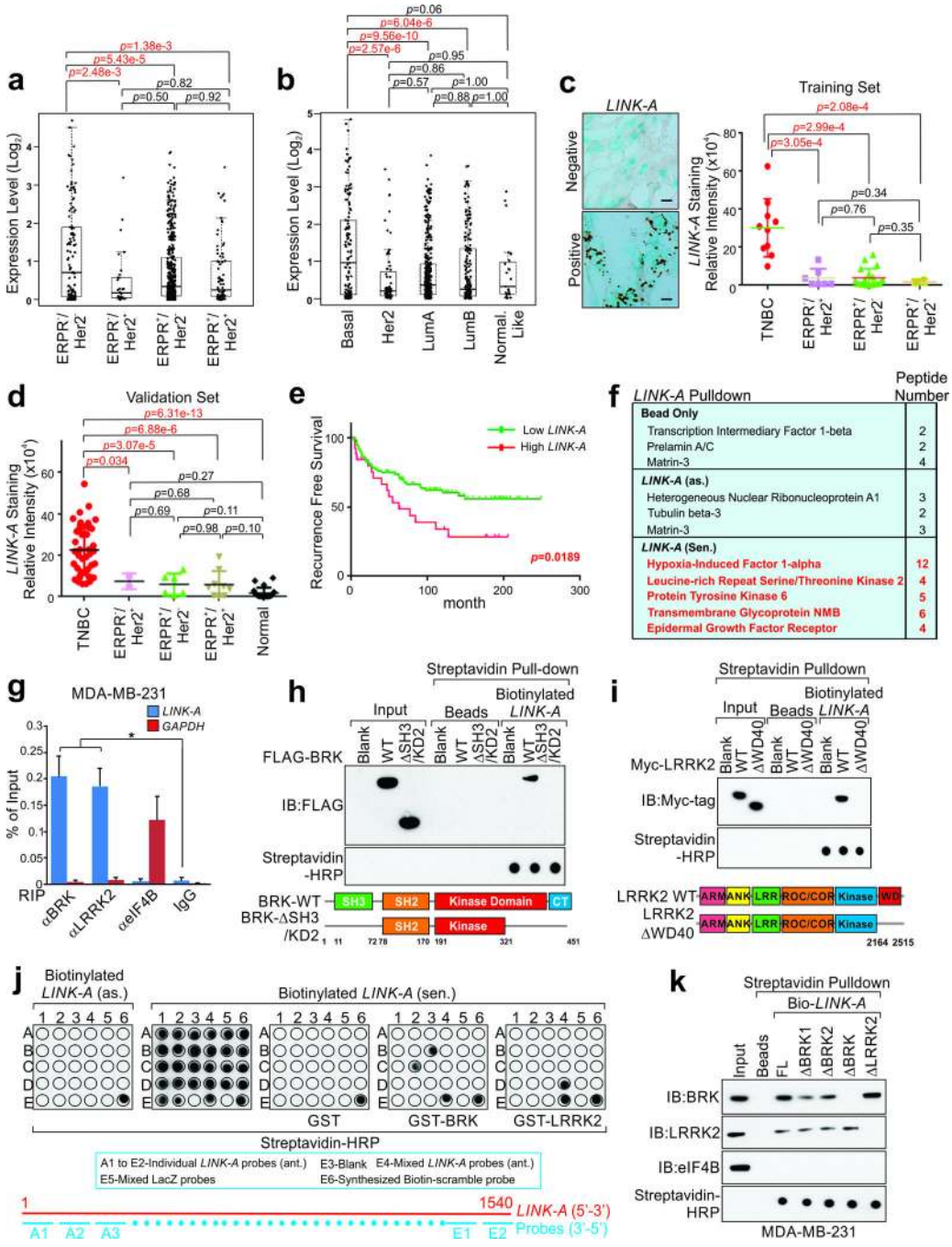

Figure 1. *LINK-A* is a TNBC-upregulated cytoplasmic lncRNA with prognostic value

(**a** and **b**) Scatter plots comparing *LINK-A* expression in breast tumors samples with different ER, PR, and HER2 status including ER−/PR−/HER2− (*n*=119), ER−/PR−/HER2+ (*n*=30), ER+/PR+/HER2- (*n*=482), and ER+/PR+/HER2+ (*n*=80) (a), or in breast tumor tissue samples with different subtype including basal (*n*=139), HER2 (*n*=67), LumA (*n*=417), LumB (*n*=191), and Normal like (*n*=23) (b). Statistical significance was determined by two-way ANOVA. The boxes show the median and the interquartile range. The whiskers show the minimum and maximum. (**c** and **d**) RNAScope® detection of *LINK-*

A expression in human breast cancer and adjacent normal tissues (training and validation set, respectively). Left panel: representative images. Scale bars, 100μm; Right panel: statistical analysis. Training set: TNBC (n=10), ER−/PR−/HER2+ (n=7), ER+/PR+/HER2- (n=18), and ER+/PR+/HER2+ (n=2); Validation set: ER−/PR−/HER2- (n=38), ER−/PR−/HER2+ (n=2), ER+/PR+/HER2- (n=6), ER+/PR+/HER2+ (n=9), and normal tissue (n=20) (median, two-way ANOVA). (**e**) Recurrence free survival analysis of *LINK-A* status in breast cancer patients detected by qRT-PCR (n=123 patients, Gehan-Breslow test). (**f**) A list of top *LINK-A*-associated proteins identified by RNA pulldown and MS analysis in MDA-MB-231 cells. (**g**) RIP-qPCR detection of indicated RNAs retrieved by BRK-, LRRK2- or eIF4B-specific antibodies in MDA-MB-231 cells. Error bars, S.E.M., n=3 independent experiments (*p<0.05, two-tailed paired Student's t-test). (**h** and **i**) *In vitro* RNA-protein binding assay showing the interaction of biotinylated *LINK-A* with wild-type (WT) FLAG-tagged BRK and deletion mutants (h), or WT Myc-tagged LRRK2 and deletion mutant (i). Dot-blot of RNA-protein binding samples indicates equal RNA transcript present in the assay. Bottom panel: graphic illustration of BRK or LRRK2 domain deletion mutants. (**j**) Upper panel: *In vitro* RNA-protein binding followed by dot-blot assays using biotinylated *LINK-A* sense (sen.) or anti-sense (as.) transcripts and GST-tagged, bacterially expression BRK or LRRK2 proteins. The hybridized RNA fragments were detected by Streptavidin-HRP. Bottom panel: graphic illustration of *LINK-A* probes. (**k**) Immunoblot (IB) detection of proteins retrieved by *in vitro* transcribed biotinylated *LINK-A* full-length (FL) or deletion mutants expressed in MDA-MB-231 cells. Unprocessed original scans of blots are shown in Supplementary Fig. 7.

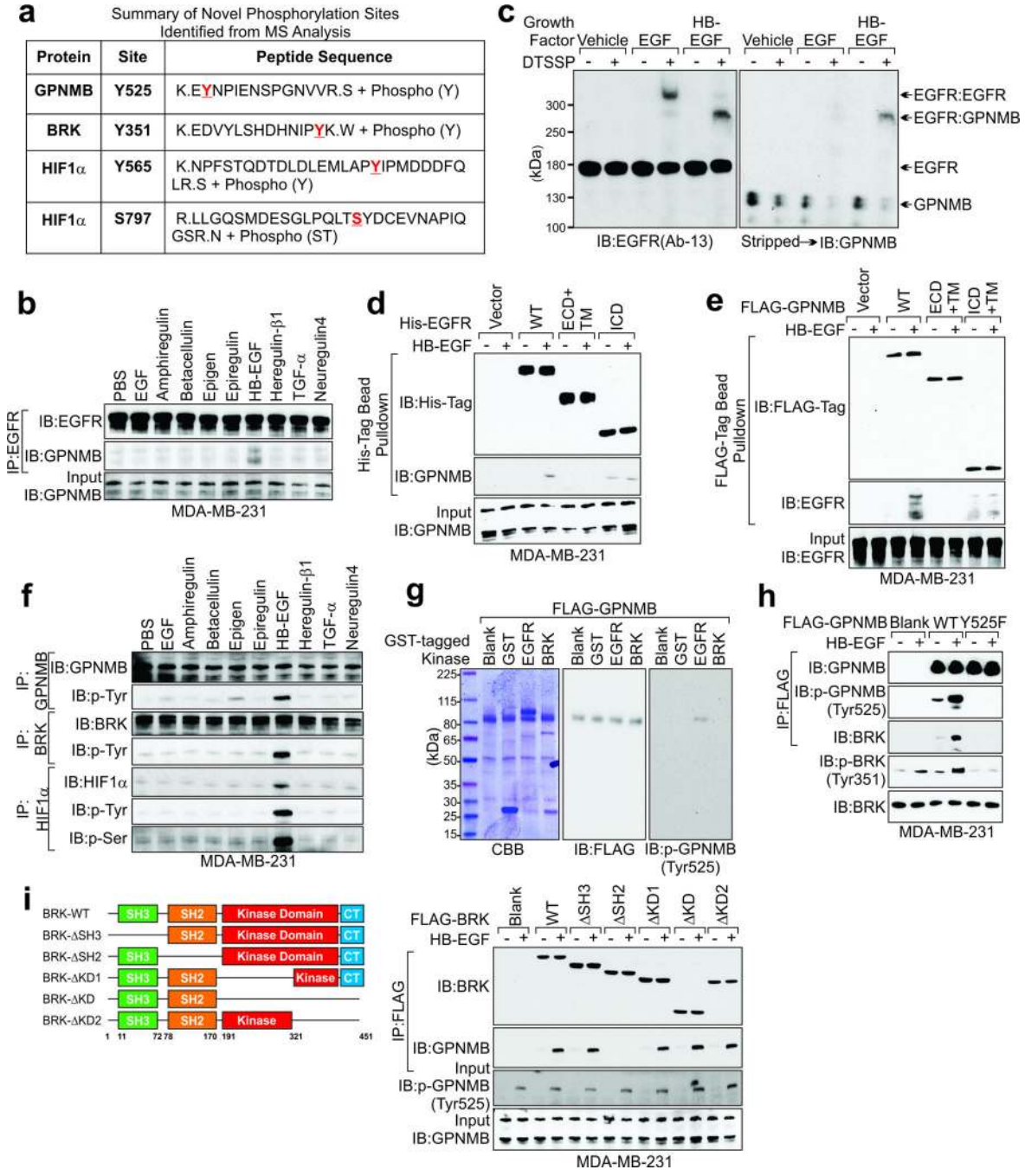

Figure 2. *LINK-A* is involved in a HB-EGF-triggered, EGFR:GPNMB-mediated signaling pathway

(**a**) Summary of phosphorylation sites of indicated proteins identified from RNA pulldown followed by MS analysis. (**b**) IP followed by IB detection of indicated proteins in MDA-MB-231cells treated with indicated growth factors for 30 min. (**c**) IB detection using indicated antibodies in MDA-MB-231 cells stimulated with vehicle, EGF or HB-EGF followed by DTSSP chemical crosslinking (1mM, 30 minutes). (**d** and **e**) His tag (d) or FLAG tag (e) pulldown followed by IB detection using indicated antibodies in MDA-

MB-231 cells transfected with indicated expression vectors followed by HB-EGF stimulation. ECD: extracellular domain; TM: transmembrane domain; ICD: intracellular domain. (**f**) IP followed by IB detection of GPNMB, BRK, and HIF1α phosphorylation in MDA-MB-231 cells treated with indicated growth factors. (**g**) *In vitro* kinase assay using indicated recombinant proteins, followed by Coomassie blue staining (CBB), and IB detection using indicated antibodies. (**h** and **i**) IP followed by IB detection using indicated antibodies in cells transfected with indicated expression vectors followed by HB-EGF stimulation. Left panel (i): graphic illustration of BRK domain deletion mutants. Unprocessed original scans of blots are shown in Supplementary Fig. 7.

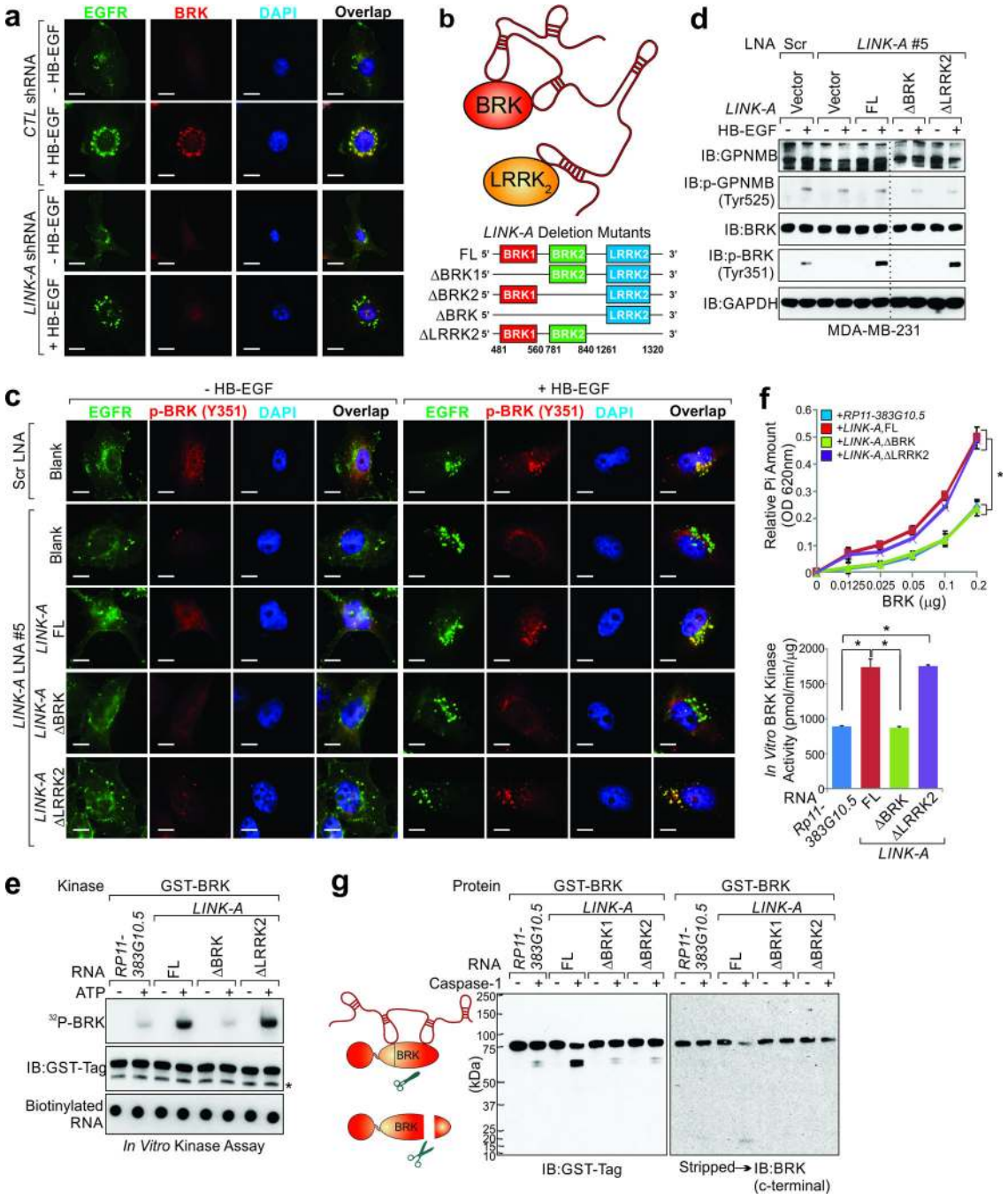

Figure 3. *LINK-A* mediates recruitment of BRK to GPNMB for kinase activation

(**a**) Immunofluorescence detection using indicated antibodies in MDA-MB-231 cells harboring control (upper panel) or *LINK-A* shRNA, followed by HB-EGF stimulation (upper panel). Scale bars, 20μm. (**b**) Graphic illustration of the BRK-, LRRK2-*LINK-A* interactions (upper panel) and corresponding deletion abolishing these interactions (lower panel). (**c** and **d**) Immunofluorescence imaging (c, Scale bars, 20μm) or IB detection (d) was performed using indicated antibodies in MDA-MB-231 cells transfected with LNA against *LINK-A* followed by overexpression of indicated rescue plasmids with HB-EGF

stimulation. (**e**) *In vitro* kinase assay using recombinant BRK and *in vitro* transcribed RNA transcripts as indicated in the presence or absence of [^{32}P]-ATP. Dot-blot indicates equal RNA transcript present in the assay. (**f**) Quantification analysis of BRK kinase activity in the presence of indicated *in vitro* transcribed RNA transcripts using HIF1α peptide (a.a. 557–566) as substrate. Upper panel: release of free Pi amount measured at OD620; lower panel: calculation of BRK kinase activity (pmol/min/μg). Error bars, S.E.M., n=3 independent experiments (*p<0.05, two-tailed paired Student's t-test) (**g**) IB detection of BRK using indicated antibodies in the presence of indicated lncRNA transcripts with or without Caspase-1 digestion. Left panel: graphic illustration of Caspase-1-mediated BRK cleavage in the absence or presence of lncRNA. Unprocessed original scans of blots are shown in Supplementary Fig. 7. The dotted line on the blots of Fig. 3d indicates the position where the images of single blots were vertically cropped to juxtapose non-adjacent lanes. The uncropped blots are shown in Supplementary Fig. 7.

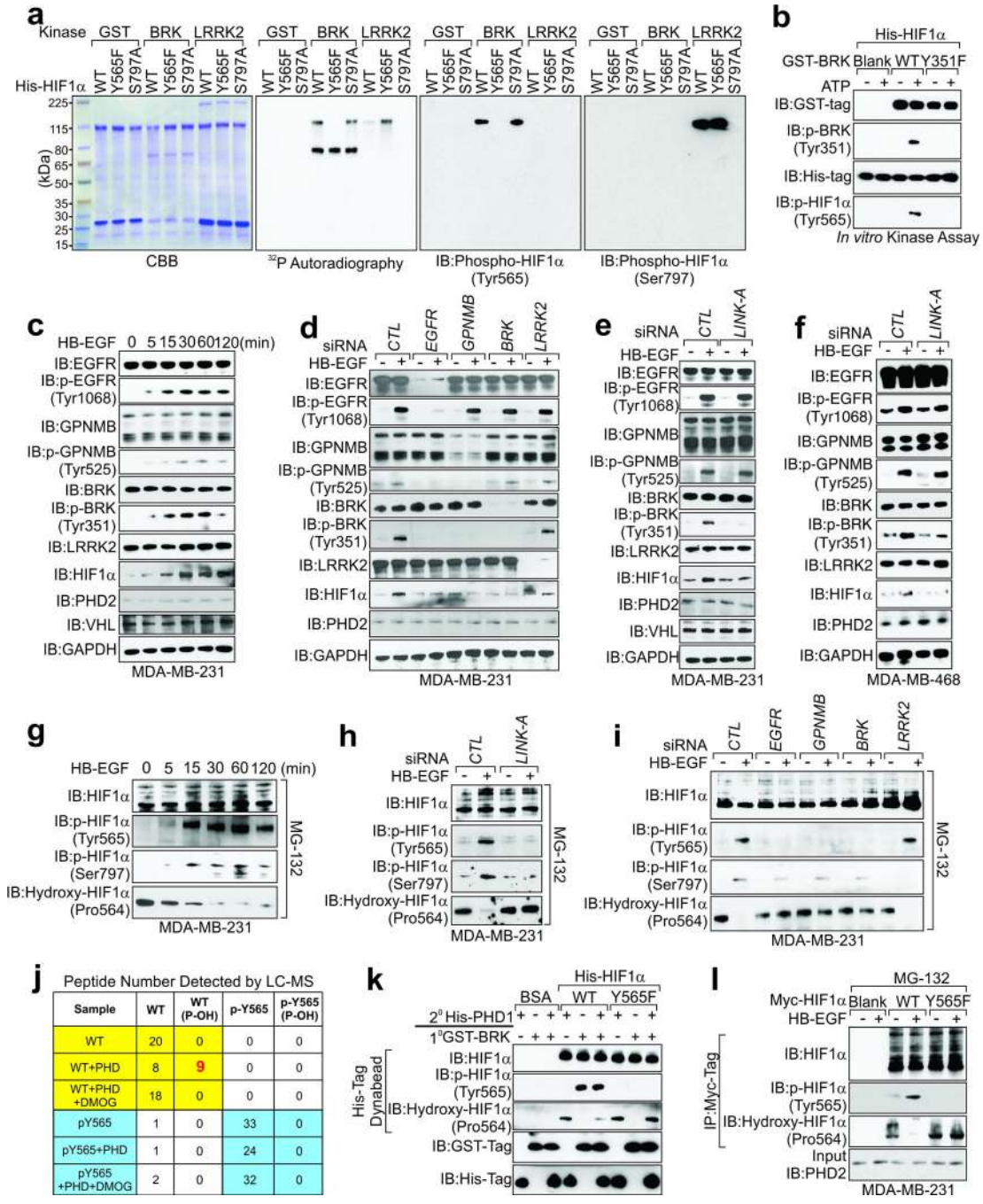

Sample	WT	WT (P-OH)	p-Y565	p-Y565 (P-OH)
WT	20	0	0	0
WT+PHD	8	9	0	0
WT+PHD +DMOG	18	0	0	0
pY565	1	0	33	0
pY565+PHD	1	0	24	0
pY565 +PHD+DMOG	2	0	32	0

Figure 4. *LINK-A*-dependent BRK phosphorylation of HIF1α at Tyr565 antagonizes HIF1α Pro564 hydroxylation

(**a**) *In vitro* phosphorylation assay using recombinant proteins (WT or mutants as indicated). (**b**) *In vitro* kinase assay using bacterially expressed GST-tagged BRK WT or mutant and His-tagged HIF1α. (**c–f**) IB detection using indicated antibodies in MDA-MB-231 (c–e) or MDA-MB-468 (f) cells treated with HB-EGF at indicated time point (c) or transfected with indicated siRNAs followed by HB-EGF treatment (d–f). (**g–i**) IB detection using indicated antibodies in MDA-MB-231 cells treated with MG-132 followed by HB-EGF treatment at

indicated time (g) or in cells transfected with indicated siRNAs followed by MG-132 and HB-EGF treatment (h and i). (**j**) LC-MS sequencing of HIF1α peptide (557–566) in *in vitro* hydroxylation assay. The total peptide number indicating proline nonhydroxylated *vs.* hydroxylated (P-OH) detected by LC-MS were shown. The peptide number of hydroxylated WT peptide was indicated as red. (**k**) His tag pulldown followed by IB detection of HIF1α phosphorylation and hydroxylation (WT *vs.* Y565F) in *in vitro* kinase assay (1°) followed by *in vitro* hydroxylation assay (2°). (**l**) IP followed by IB detection of HIF1α phosphorylation and hydroxylation (wt *vs.* Y565F) in MDA-MB-231 cells transfected with indicated plasmids and treated with MG-132 followed by HB-EGF treatment. Unprocessed original scans of blots are shown in Supplementary Fig. 7.

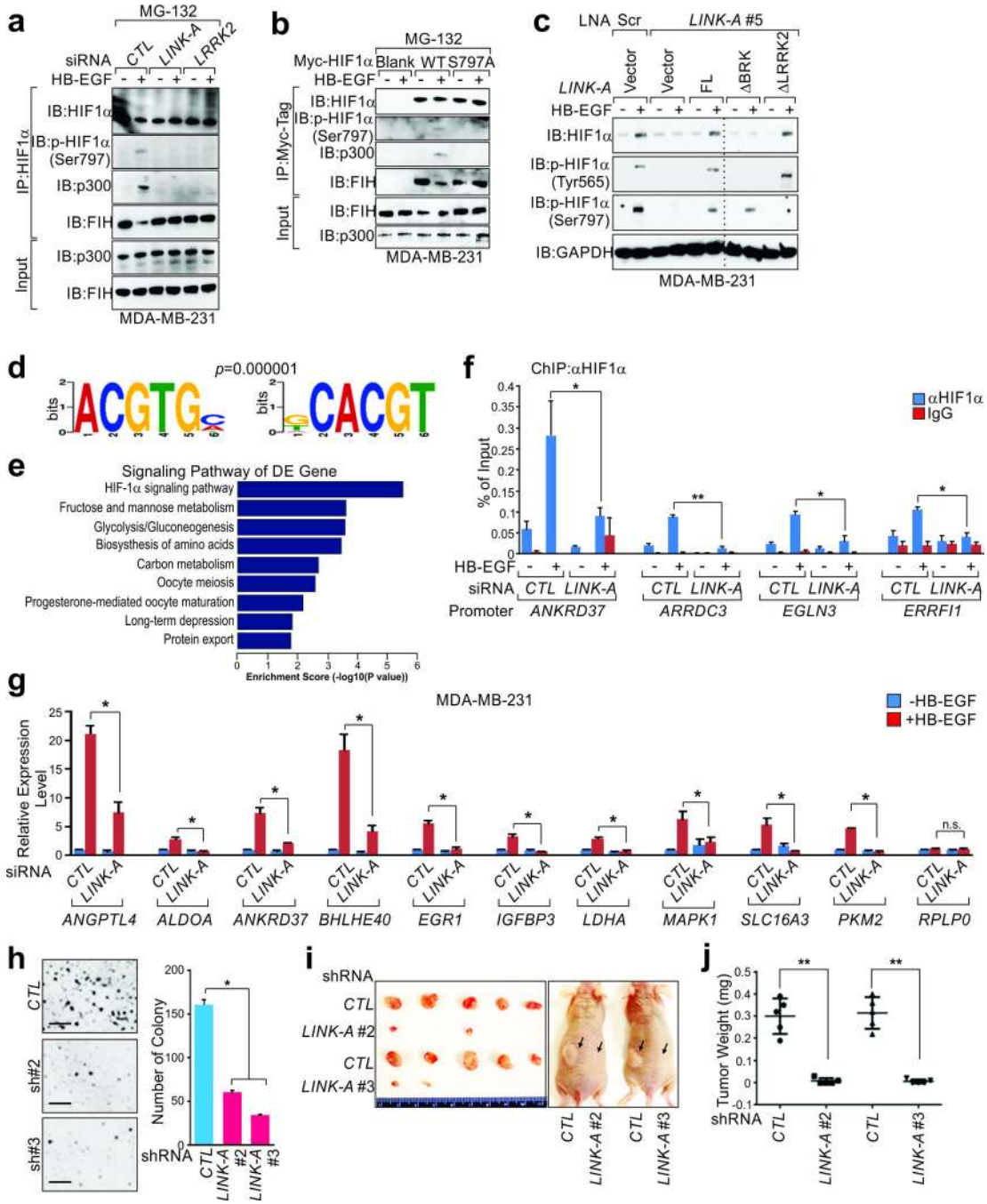

Figure 5. *LINK-A*-recruited LRRK2 phosphorylates HIF1α at Ser797, enhances HIF1α transcriptional activity and promotes tumor growth

(**a** and **b**) IP followed by IB detection using indicated antibodies in MDA-MB-231 cells transfected with indicated siRNAs (a) or plasmids (b), and treated with MG-132 followed by HB-EGF treatment. (**c**) IB detection using indicated antibodies in MDA-MB-231 cells transfected with LNA against *LINK-A* followed by overexpression of indicated rescue plasmids and HB-EGF stimulation. (**d**) HIF1α ChIP-seq analysis showing top enriched HIF binding consensus motifs. (**e**) HIF1α ChIP-seq analysis showing signaling pathways in

MDA-MB-231 cells treated with HB-EGF. (**f** and **g**) ChIP-qPCR detection of HIF1α occupancy on indicated target gene promoters (f) and qRT-PCR analysis of HIF1α target genes expression (g) in MDA-MB-231 cells transfected with control or *LINK-A* siRNA followed by HB-EGF treatment. (**h**) Colony formation assay in MDA-MB-231 cells transduced with control and *LINK-A* shRNAs. Scale bars, 200μm. For panel **f**–**h**, error bars, S.E.M., n=3 independent experiments (*p<0.05 and **p<0.01, two-tailed paired Student's t-test). (**i** and **j**) *In vivo* analyses of tumor growth (i) or weight (j) in mice that were subcutaneously injected with MDA-MB-231 cells harboring control or *LINK-A* shRNA. Data are mean±S.E.M., n=5 mice *per* group (**p<0.01, two-tailed paired Student's t-test). Unprocessed original scans of blots are shown in Supplementary Fig. 7. The dotted line on the blots of Fig. 5c indicates the position where the images of single blots were vertically cropped to juxtapose non-adjacent lanes. The uncropped blots are shown in Supplementary Fig. 7.

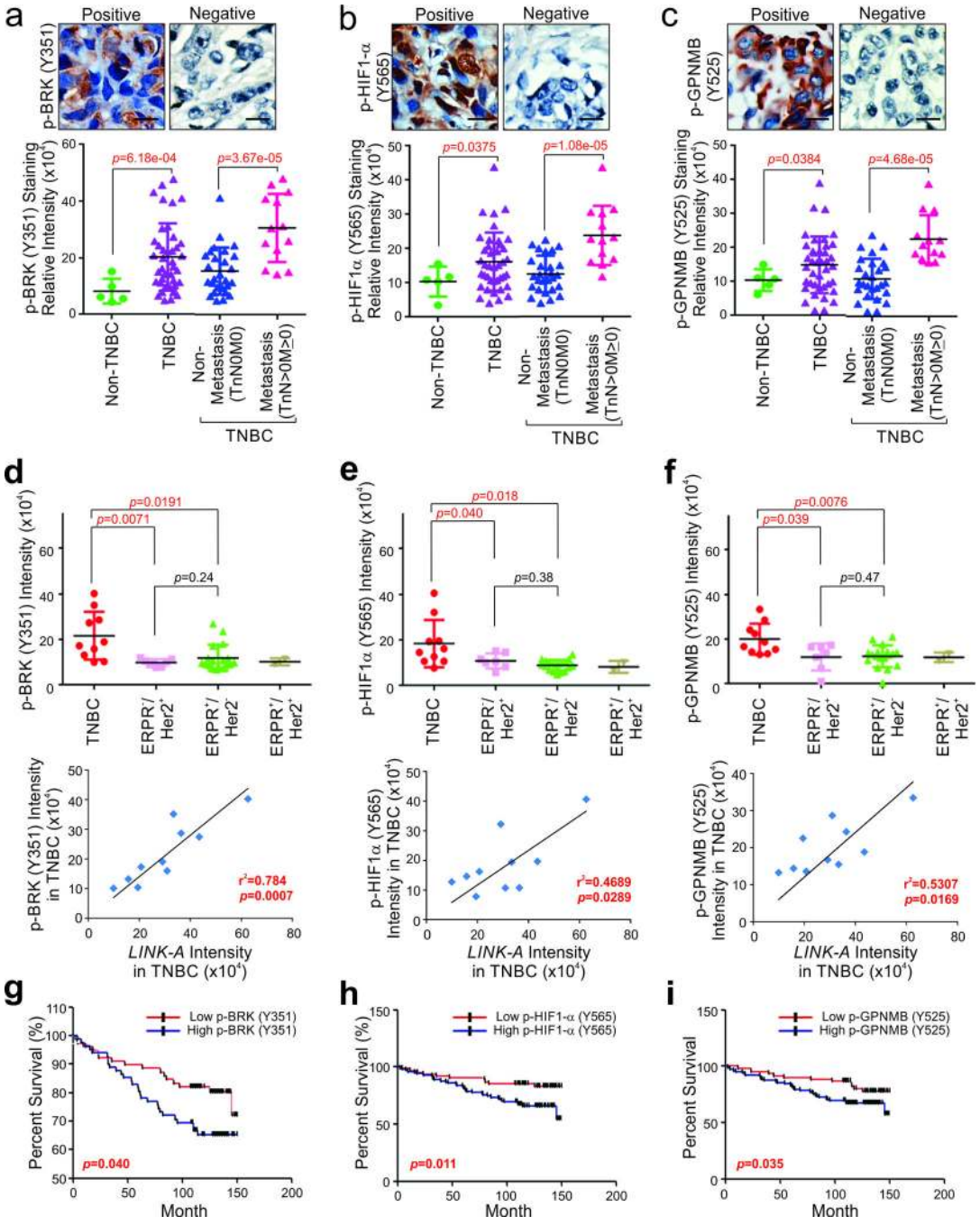

Figure 6. *LINK-A*-dependent normoxic HIF1α signaling pathway correlates with TNBC

(**a–c**) Immunohistochemical staining using antibodies against phospho-BRK (Tyr351) (a), phospho-HIF1α (Tyr565) (b), or phospho-GPNMB (Tyr525) (c) in human breast cancer tissues. Upper panel: representative image. Scale bars, 100μm; Lower panel: statistics analysis based on non-TNBC tissues (*n*=5) *vs.* TNBC tissues (*n*=40) and non-Metastasis (TnN0M0) TNBC (*n*=27) *vs.* Metastasis (TnN>0M>0) breast tissues (*n*=13) (median, two-way ANOVA). (**d–f**) Upper panel: statistical analysis of immunohistochemical staining using antibodies against phospho-BRK (Tyr351) (d), phospho-HIF1α (Tyr565) (e) or

phospho-GPNMB (Tyr525) (f) in human breast cancer tissues including TNBC (n=10), ER −/PR−/HER2+ (n=7), ER+/PR+/HER2- (n=18), and ER+/PR+/HER2+ (n=2) (median, two-way ANOVA). Lower panel: Pearson's correlation analysis comparing staining density between *LINK-A* expression and phospho-BRK (Tyr351) (d), phospho-HIF1α (Tyr565) (e), or phospho-GPNMB (Tyr525) (f) within the TNBC group (n=10 tissue samples, Fisher's exact test). (**g–i**) Kaplan-Meier survival analysis of phosphor-BRK (Tyr351) (g), phosphor-HIF1α (Tyr565) (h), and phospho-GPNMB (Tyr525) (i) status in breast cancer patients (n=160, Gehan-Breslow test).